Fuel 334 (2023) 126750

Contents lists available at ScienceDirect

Fuel

journal homepage: www.elsevier.com/locate/fuel

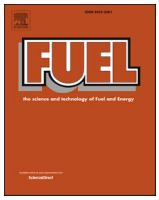

Full Length Article

Smoldering peat fire detection by time-resolved measurements of transient CO_2 and CH_4 emissions using a novel dual-gas optical sensor

Mohsin Raza [a,1], Yuying Chen [b,1], Joshua Trapp [a], Haojia Sun [a], Xinyan Huang [b,*], Wei Ren [a,*]

[a] Department of Mechanical and Automation Engineering, and Shenzhen Research Institute, The Chinese University of Hong Kong, New Territories, Hong Kong SAR, China

[b] Research Centre for Fire Safety Engineering, Department of Building Environment and Energy Engineering, The Hong Kong Polytechnic University, Hong Kong SAR, China

ARTICLE INFO

Keywords:
Absorption spectroscopy
Wavelength modulation spectroscopy
Smoldering combustion
Peat fire emission
CO_2 and CH_4 gas monitoring

ABSTRACT

A compact and sensitive dual-gas laser absorption sensor was developed for smoldering peat fire detection by real-time monitoring of transient CO_2 and CH_4 emissions from peat combustion exhaust. The sensor combines two infrared lasers to exploit CH_4 and CO_2 absorption lines centered at 6057.09 cm^{-1} and 6359.96 cm^{-1}, respectively. Scanned-wavelength modulation spectroscopy with the second-harmonic detection (WMS-2*f*) and a custom-designed Herriot multipass gas cell (10.3 m path length in a 40.5 mL volume) were employed to improve detection sensitivity. The simultaneous real-time transient emissions (CH_4 and CO_2) were measured at an interval of 0.1 s under various smoldering peat combustion conditions in a top open cylindrical reactor. An increasing trend of CH_4/CO_2 ratio from 0.053 to 0.075 and the greenhouse gas (GHG) flux from 1.5 g/m^2 s to 3.4 g/m^2 s was observed with increasing oxygen supplies from 10 mm/s to 24 mm/s. However, a decreasing trend of CH_4/CO_2 ratio from 0.06 to 0.043 and GHG flux from 2.6 g/m^2 s to 0.4 g/m^2 s was noticed with increasing peat moisture content from 8% (dry peat) to 100%. The measurement results agree well with commercial non-dispersive infrared CO_2 and CH_4 analyzers which are not fast enough to capture transient emissions due to their low time response. The developed dual-gas sensor has the potential to be applied for detecting underground peatland fires and evaluating the overall GHGs emissions from smoldering wildfires due to its excellent temporal resolution, hardware simplicity, and compactness.

1. Introduction

Smoldering is the slow, low-temperature, and flameless burning of porous fuels and one of the most persistent types of combustion phenomena [1]. Smoldering peat fires are the largest wildfires on Earth (in terms of fuel consumption) that irreparably degrade soil ecosystems [2]. The global smoldering peat fires release massive greenhouse gases (GHGs), mainly carbon dioxide (CO_2) and methane (CH_4) as reported in the literature [3–5], which is equivalent to 10–15% of man-made emissions and comparable to the total emissions from the European Union [6,7]. Measuring the concentrations of these two primary GHGs (CH_4 and CO_2), as well as their ratio, can help detect smoldering peat fires and estimate fire intensity. Compared to flaming wildfires [3,8], smoldering wildfires generate more unburnt hydrocarbons and toxic gases [9,10], but relatively few studies focus on the dynamic emissions from smoldering. This work aims to develop new methods and sensors for detecting smoldering peat fires by measuring transient CO_2 and CH_4 emissions, which helps pave the way for studying real peatland fires.

Several commercially available instruments including metal oxide semiconductor sensors, non-dispersive infrared (NDIR) sensors, gas chromatography-mass spectrometry (GC–MS), and Fourier transform infrared (FTIR) spectroscopy have been used for CH_4 and CO_2 monitoring in combustion systems and process industrial units. Metal oxide semiconductor gas sensors are compact, lightweight, and offer a quick response time (<1 min), and high sensitivity (ppm-level), but they need a high temperature for operation and their performance is affected by humidity [11]. NDIR sensors have been widely used for monitoring GHGs emissions [12–15], but they suffer from low sensitivity, poor selectivity, and instability [16]. GC–MS and FTIR have been used for analyzing smoldering combustion emissions [17–19]. GC–MS can be

* Corresponding authors.
E-mail addresses: xy.huang@polyu.edu.hk (X. Huang), renwei@mae.cuhk.edu.hk (W. Ren).
[1] These authors contributed equally.

https://doi.org/10.1016/j.fuel.2022.126750
Received 23 June 2022; Received in revised form 18 October 2022; Accepted 12 November 2022
Available online 24 November 2022

used to analyze complex gas mixtures due to its advantages of temporal separation of molecules [20]. However, it reduces the possibility of real-time measurements due to the long analysis time up to tens of minutes required for the gas mixture to be separated in the capillary column [21]. Furthermore, the high cost, bulky size, and heavy weight limit its wide applications. FTIR spectrometer has been employed for multi-component analysis with a wide spectral coverage [22], but it suffers from slow response time, high cost, and bulky size.

Tunable diode laser absorption spectroscopy (TDLAS) is a powerful trace gas sensing technology compared to the above-mentioned methods, which offer highly sensitive, accurate, quantitative, and species-specific measurements as well as robust and compact sensor systems [23–25]. The advantage of short response time makes it particularly suitable for online real-time gas process control and combustion exhaust monitoring applications. TDLAS sensors have been widely used for GHG sensing and exhaust gas monitoring in industrial combustion systems. However, their applications for smoldering combustion research have been scarcely reported. Hangauer et al. developed a 2.3 μm CO sensor using vertical-cavity surface-emitting lasers (VCSELs) for smoldering wood fire detection [26]. They achieved sub-ppm level of CO detection with a time resolution of 1 min. Fallows et al. demonstrated a portable cavity ringdown spectrometer for detecting smoldering cigarettes fire [27], and successfully detected a peak concentration of 270 ppm CO, 2100 ppm CO_2, and 310 ppb C_2H_2.

Smoldering cigarette fire has also been detected by measuring nitric oxide (NO) using a 5.24 μm quantum cascade laser (QCL) [28]. The detection limit of 28 ppb over 180 s integration time was achieved using a single-pass absorption cell with an effective path length of 1 m. Qiu et al. demonstrated a 2.3 μm distributed feedback laser-based CO sensor for smoldering fire detection using scanned-WMS combined with a Herriot-type multipass cell (19.98 m effective path length) [29]. The above literature reveals that earlier research studies have not reported the smoldering peat fire detection by measuring emission gases with the state-of-the-art TDLAS-based sensors. Hence, their potential for smoldering combustion and wildfires is valuable to be explored.

In this work, a compact and sensitive dual-gas sensor was designed based on time-division multiplexed scanned-WMS-2*f* for detecting peat fire by real-time monitoring of transient CH_4 and CO_2 in the smoldering peat combustion exhaust. The developed sensor can simultaneously detect CH_4 and CO_2 by targeting the selected lines peaked at 6057.09 cm^{-1} and 6359.9 cm^{-1}, respectively. These transition lines present in the near-infrared region have relatively weak absorption strength compared to strong absorption lines in the mid-infrared region [30,31]. However, the current mid-infrared laser sources are not widely used for field applications due to their high cost. To obtain a higher detection sensitivity using the near-infrared lasers, a custom-designed multipass gas cell (effective path length greater than 10 m in a 40.5 mL volume) was employed for developing a highly sensitive and inexpensive dual gas detector. The sensor performance was evaluated in terms of its stability, measurement precision, and detection limit in the laboratory. The developed sensor was applied for real-time monitoring of CH_4 and CO_2 from the exhaust of a lab-scale smoldering combustion reactor.

2. Time-division multiplexing laser absorption spectroscopy

The principle of laser-based absorption spectroscopy has been comprehensively explained previously [32], thus a brief description is presented here to establish notation. The foundation of laser absorption spectroscopy is the Beer-Lambert relation which relates the interaction of monochromatic light and uniform gas-phase atoms or molecules as described in Eq (1):

$$\tau(v) = (I_t/I_0)_v = exp(-\alpha_v) = exp(-S(T)\phi_v XPL) \quad (1)$$

where incident and transmitted laser intensities are represented by I_o and I_t, respectively, α_v is the spectral absorbance, ϕ_v refers to the line-shape function, $S(T)$ (cm^{-2} atm^{-1}) is the line-strength of the transition at temperature T (K), *X*, *L,* and *P* represents the mole fraction, optical path length, and total gas pressure, respectively.

Scanned-WMS-2*f* detection scheme is preferred for trace gas detection with a relatively small amount of absorbance [23]. The nominal wavelength of a tunable diode laser is usually scanned across the absorption line of the target species with a slow (Hz) sawtooth or triangular injection current. An additional sinusoidal modulation at fast (kHz) frequency *f* applies to the slower scan current. The laser output frequency can be described by Eq. (2):

$$v(t) = \bar{v}_{-}(t) + a\cos(2\pi ft) \quad (2)$$

where $\bar{v}_{-}$ (cm^{-1}) is the laser-center frequency and a (cm^{-1}) is the modulation depth. The laser intensity I_o is modulated simultaneously while tuning the laser injection current:

$$I_o(t) = \bar{I}_{o\,-}[1 + i_1\cos(2\pi ft + \psi_1) + i_2\cos(2\pi ft + \psi_2)] \quad (3)$$

where $\bar{I}_{o\,-}$ is the average laser intensity, i_1 and i_2 are the linear and nonlinear laser intensity modulation amplitudes, respectively; ψ_1 and ψ_2 are the linear and nonlinear phase shifts between the laser intensity modulation and wavelength modulation. As the laser output frequency ν is modulated, the fractional transmission τ as a function of ν becomes a periodic function at *f*. Thus, the transmitted laser intensity measured by the detector can be expanded by a Fourier series:

$$I_t(t) = I_o(t).\tau(\nu(t)) = \bar{I}_o[1 + i_1 cos(2\pi ft + \psi_1 f) + i_2 cos(2\pi ft + \psi_1 f)].\left[\sum_{k=0}^{\infty} H_k cos(k.2\pi ft)\right] \quad (4)$$

where H_k is the *kth* order Fourier harmonic coefficient that contains the absorption information [33]. Under the optical-thin condition, H_k is linearly proportional to the gas concentration. Thus, the target gas concentration can be derived from the measured harmonic signal if other properties of the target gas are known.

In the scanned-WMS-2*f* scheme, high-frequency modulation is added in the laser injection current to raise the signal detection band to the designated higher frequency range, which eliminates the low-frequency noise in practical measurements and thus significantly increases the signal-to-noise ratio (SNR). A lock-in amplifier (LIA) is used to extract the 2*f* component which multiplies the measured photodetector laser intensity signal with the reference sinusoid at 2*f* and shifts the harmonic component to DC. Then a low-pass filter is employed to isolate the DC signal and reject other noise beyond the filter passband. Therefore, the scanned-WMS-2*f* technique usually merits a larger SNR under noisy environmental conditions and is particularly suitable for trace gas sensing in the field.

Time-division multiplexing (TDM) is an effective method used for multispecies gas sensing due to its advantages of simpler hardware and data processing [34]. In the TDM-WMS technique, each laser is switched on in succession, resulting in a detector signal that is composed of each laser signal in sequence. Both lasers are modulated at different modulation frequencies but scanned at the same scanning frequency to target the absorption lines. A sequence chart of an individual (1572 nm CO_2 laser, 1654 nm CH_4 laser) and combined time-division multiplexed dual-lasers WMS signal is shown in Fig. 1. In this work, the selected CO_2 and CH_4 absorption transitions were exploited by scanning the laser's wavelength at 10 Hz along with fast sinusoidal modulation frequencies of 15 kHz and 18 kHz, respectively. The measurements were completed every 200 ms by activating lasers in turn of 100 ms. One photodetector was used to record absorption signals and then pass through digital lock-in amplifiers to obtain the second harmonic WMS (WMS-2*f*) signals.

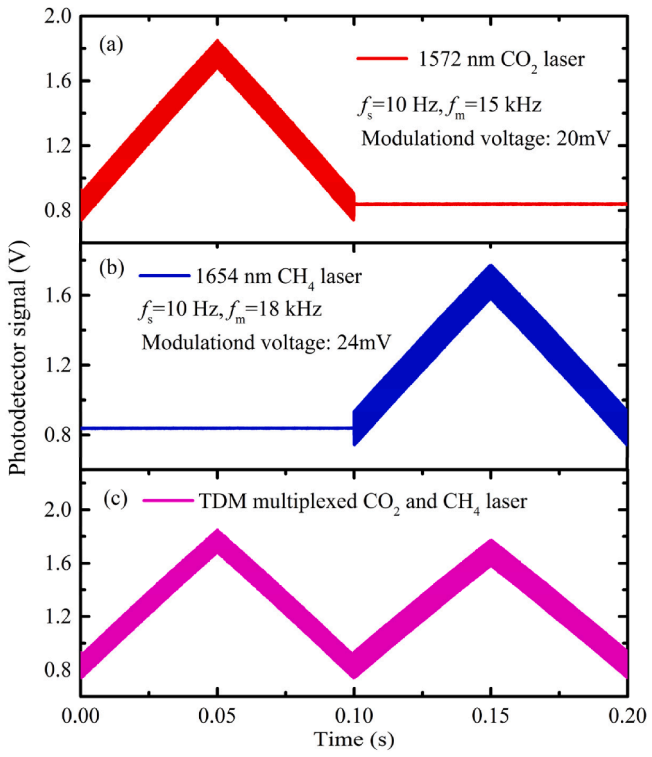

Fig. 1. Sequence chart of measured photodetector signals for (a) CO_2 at 1572 nm, (b) CH_4 at 1654 nm, and (c) combined time-division multiplexed dual-laser.

3. Experimental methods

3.1. Absorption line selection

The performance and accuracy of laser absorption sensors can be significantly improved by carefully selecting the absorption line. In Fig. 2, the line strength is shown in the near-infrared range of 5603–6059 cm^{-1} for CH_4 and 6350–6420 cm^{-1} for CO_2. The spectral lines of 6057.09 cm^{-1} for CH_4 and 6359.9 cm^{-1} for CO_2 were chosen due to their strong absorption, spectral isolation from the nearby transitions, and coverage within a single laser scan range. Two NIR distributed feedback diode lasers (1650 nm for CH_4 and 1572 nm for CO_2) were employed to target the selected absorption lines. A spectrum analyzer (Bristol Instruments) was utilized to characterize both lasers. The linear relation between the laser injection current and wavenumber is shown in Fig. 2. The 1650 nm DFB laser was scanned across the target CH_4 line by changing the laser current between 40 and 100 mA at 27 °C laser temperature while the 1572 nm laser exploited the CO_2 line by setting the laser temperature to 25 °C and varying the injection current between 35 and 95 mA.

3.2. Sensor system configuration

Fig. 3 (a) depicts the dual-gas sensor system comprised of two near-infrared distributed feedback (DFB) diode lasers with 14-pin butterfly packages (Wuhan Liujiu ltd.), low-noise laser drivers (Wavelength Electronics ltd.), a custom-made multipass gas cell (MGC), and gas-handling equipment. A LabVIEW-based function generator was used to control both laser's modulation currents. The transmitted laser intensity signal was transformed from the time domain to the frequency domain using a silicon etalon with a free spectral range of 0.0834 cm^{-1}.

In this work, a customized mini-Herriot-type MGC with a 10.3 m path length in a 40.5 mL volume was employed. It was composed of two 1-inch diameter spherical mirrors. The spherical concave mirrors were designed by using Zemax software as explained in Ruyue et al. [36]. A wavelength beam combiner was used to combine both CH_4 (1650 nm) and CO_2 (1572 nm) laser beams. The seven nonintersecting-circle spot patterns on both mirrors was accomplished by coupling the combined laser beam into the MGC as illustrated in Fig. 3 (a). The laser beam exiting the MGC was focused on an infrared photodetector (PDA20CS2, Thorlabs) by a 50 mm focal lens.

The gas-handling system, which included mass flow controllers, a mixing tank, and compressed CO_2, CH_4, and N_2 gas cylinders, was connected to the mini-MGC to calibrate the dual-gas sensor. Mass flow controllers were used to control the flow rate of the target gases, which were mixed in a tank and then filled into the cell for measurements.

3.3. Lab-scale smoldering fire test

Peat soil was chosen as a representative fuel that is prone to smoldering combustion. Before the test, the peat sample was oven-dried at 90 °C for 48 h. The bulk density of the dried peat sample was measured to be 145 ± 10 kg/m^3. The proximate analysis shows 70.8%, 23.5%, and 5.7% mass fractions for volatile matters, fixed carbon, and ash, respectively. The element analysis of the wood sample shows 46.09%, 5.75%, 47.46%, 0.47%, and 0.23% mass fractions for C, H, O, N, and S, respectively. To obtain different moisture contents, the dried peat was then well mixed with the corresponding amount of water. The schematic

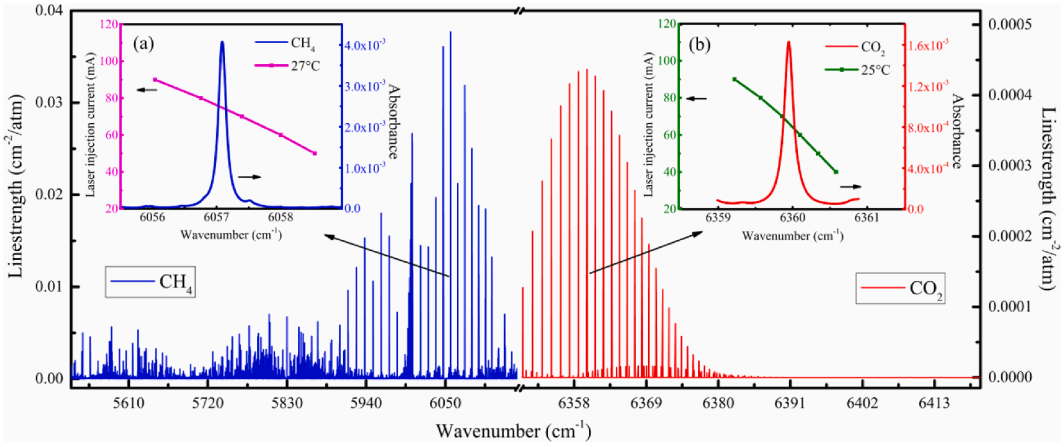

Fig. 2. Spectral line strength in the near-infrared range of 5603–6059 cm^{-1} for CH_4 and 6350–6420 cm^{-1} for CO_2 (HITRAN database) [35]. Inset graphs: wavenumber variation of (a) 1650 nm laser and (b) 1572 nm laser with the laser injection current, along with the simulated absorption spectra of 9 ppm CH_4 and 850 ppm CO_2 at 1 atm, 300 K, and an absorption length of 10.3 m.

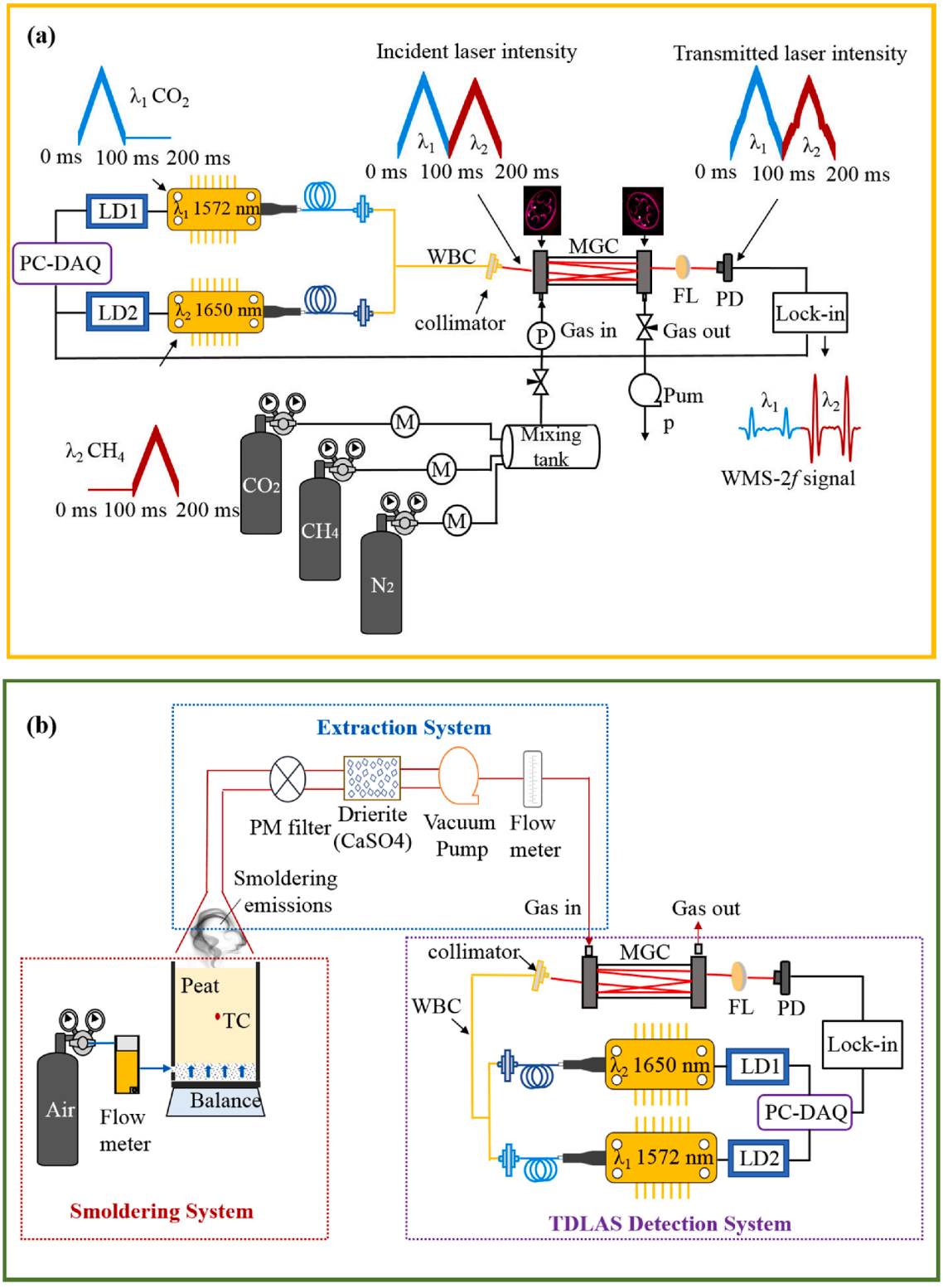

Fig. 3. (a) Schematic of the dual-gas (CH_4 and CO_2) sensor system. PD: photodetector; LD: laser driver; WBC: wavelength beam combiner; P: pressure sensor; M: mass flow controller; FL: focusing lens; MGC: multipass gas cell. (b) Schematic diagram of the experimental setup for the time-resolved laser absorption measurements of CO_2 and CH_4 in smoldering combustion exhaust.

diagram of the experimental setup for time-resolved laser absorption measurements of CO_2 and CH_4 in smoldering combustion exhaust is shown in Fig. 3 (b). It includes a smoldering system, an extraction system, and the TDLAS detection system. The smoldering system consists of a small top-open cylindrical reactor and forced air supply devices. A sample with a controlled volume was filled into the reactor with a height of 10 cm. A forced airflow was supplied from the bottom of the reactor, and the flow rate was controlled by the flow meter. To monitor the smoldering temperature, a K-type thermocouple was inserted into the fuel sample with its bead at the center of the reactor. The electrical

balance (PS 10100.R2, RADWAG) with a maximum measuring range of 10100 g and a precision of 0.01 g was used for weighing the mass loss of the peat during smoldering combustion.

The smoldering combustion was initiated by the lighter with a flame for 2 min, which was strong enough to generate a robust smoldering. A forced airflow was supplied after ignition. We controlled two parameters in the smoldering system such as the airflow velocity (u_{air} = 10 mm/s, 18 mm/s, and 24 mm/s) and the peat moisture content (MC = 8%, 50% and 100%). After the successful smoldering combustion, the smoldering exhaust gases were extracted from above the burner by a pump and entered into the MGC at a flow rate of 600 mL/min after filtering the particulate matter (PM) and drying the smoldering emissions. The transient CH_4 and CO_2 emissions were simultaneously detected by our developed TDLAS sensor.

4. Results and discussion

4.1. Sensor performance evaluation

In WMS measurements, the 2*f*-signal depends not only on line parameters such as line strength but also on the modulation depth (*a*). The optimum modulation depth needs to be selected to obtain the maximum amplitude of the 2*f*-signal. In this test, the gas mixture of 1170 ppm CH_4 and 11.05% CO_2 was filled in the MGC to measure the WMS-2*f* amplitude at different modulation depths by varying applied modulation voltages to 1650 nm laser and 1572 nm laser. The maximum amplitude 2*f*-signal for CH_4 and CO_2 was found at an optimum modulation depth of 24 mV and 20 mV, respectively, as shown in Fig. 4.

The developed dual gas sensor was first tested and calibrated in the laboratory at atmospheric pressure and room temperature. The WMS-2*f* signals of CH_4 and CO_2 with known concentrations are shown in Fig. 5 (a) and (b). The WMS-2*f* amplitude peak of measured signals as a function of known gas concentrations is plotted as a linear relationship in Fig. 5 (c) for CH_4 and (d) for CO_2. The continuous monitoring of the peak amplitude of the WMS-2*f* signal for each tested gas concentration is shown in the inset of Fig. 5 (c) for CH_4 and (d) for CO_2.

Allan-Werele deviation analysis was used to determine the sensor minimum detection limit (MDL) by measuring pure N_2. The continuous measurement was conducted for ~ 15 min by scanning the time-division multiplexed CH_4 laser (1650 nm) and CO_2 laser (1572 nm) across the target absorption lines at a 10 Hz rate. The results of Allan-Werle deviation analysis are plotted in Fig. 6 (a) for CH_4 and Fig. 6 (b) for CO_2, respectively. The MDLs of 0.82 ppm-CH_4 and 220 ppm-CO_2 were attained at 0.05-s integration time, which was then enhanced to 0.058 ppm-CH_4 and 17 ppm-CO_2 at 42-s and 27-s integration time, respectively.

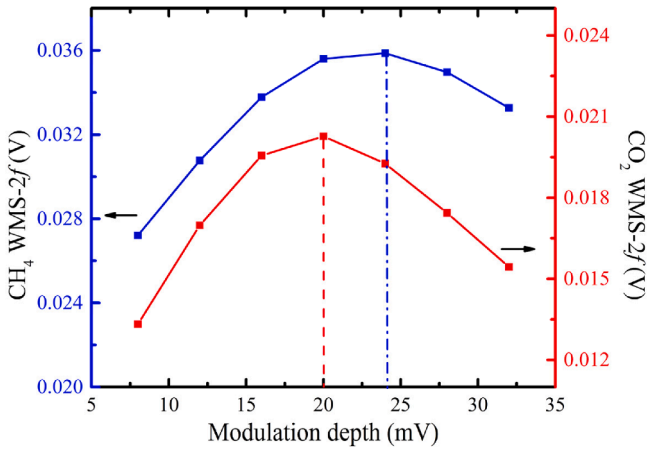

Fig. 4. Measured amplitude of 2*f* signal versus modulation depth for 1170 ppm CH_4 and 11.05% CO_2 gas mixture.

The sensor stability and precision were examined by recording the continuous time-series measurements of 9 ppm CH_4 and 850 ppm CO_2 gas mixtures as shown in Fig. 7 (a) and (b), respectively. Noise sources such as laser instability, temperature change, and mechanical vibration can influence the sensor system stability [37]. The continuous concentration measurements were recorded to evaluate the random noise level of optical measurement as shown in Fig. 7 (a) which indicates that the sensor system has good stability with little drift cause by the random noise. The frequency distributions of the continuous measurements of CH_4 and CO_2 are presented in the histogram plot in Fig. 7 (c) and (d), respectively. The measured concentration distributions of CH_4 and CO_2 can be fitted by the Gaussian profile. The half-width at half maximum (HWHM) of the Gaussian profile is determined to be 0.52 ppm for CH_4 and 56 ppm CO_2, corresponding to a precision of 5.4% (9 ± 0.52 ppm) and 6.1% (850 ± 56 ppm) at 0.1 s average time, respectively.

The uncertainties in CH_4 and CO_2 measurements were estimated to be 6.21% and 6.22%, respectively, by taking into account the optical measurement uncertainty of 5.4% for CH_4 and 6.1% for CO_2, uncertainty of the thermal-type MFC (0.7%), and line-strength uncertainty of CH_4 (3%) and CO_2 (1%) from the HITRAN database.

4.2. Smoldering emission monitoring

The performance of the TDLAS sensor was compared with the traditional commercial instruments (NDIR CO_2 and CH_4 analyzers, TSI ltd.) by conducting real-time measurements of the smoldering emissions under the airflow velocity of 10 mm/s. As shown in Fig. 8, the continuous time-series measurement results of our developed TDLAS sensor were found to be in good agreement with commercial detectors. It was noticed that the commercial NDIR CO_2 and CH_4 analyzers show a time resolution of ~ 2.5 min and ~ 3 min, respectively, which is inadequate for measuring the transient change in emission gas concentration. Additionally, these detectors were not able to detect gas concentrations below 10 ppm. However, our developed TDLAS sensor offers a quick response with a time resolution of 0.1 s. Besides, the TDLAS sensor can easily detect very low gas emissions at a few ppm levels.

As oxygen supply and fuel moisture content are two important parameters influencing smoldering combustion, we used the developed TDLAS sensor to detect the smoldering emissions under various airflow velocities and peat moisture contents. Fig. 9 shows the evolutions of the mass-loss rate, and CO_2 and CH_4 concentrations during the smoldering combustion. It should be noted that the data recording starts when the airflow is turned on, thus the ignition period is not included. As shown in Fig. 9, the evolution of the CO_2 and CH_4 concentrations follow the trend of mass loss rate of peat smoldering, indicating that the gas emissions are dependent on the oxygen supply and combustion dynamics. When the airflow velocity increases from 10 to 18 mm/s, both CO_2 and CH_4 concentrations show significant increases, which is due to the intense smoldering reaction under the enhanced oxygen supply. However, as the airflow velocity continuously increases from 18 mm/s to 24 mm/s, the CO_2 and CH_4 emissions decrease slightly instead, which agrees with the variation of the mass-loss rate. This may be caused by the non-negligible convective heat loss under an excessively large airflow of 24 mm/s. In other words, the smoldering reaction is more intense under the airflow velocity of 18 mm/s which can be verified from the larger mass loss rate in Fig. 9a, thus, causing more gas emissions to be released.

It is also observed that the CO_2 concentration is significantly larger than that of CH_4. Additionally, CO_2 is emitted for a slightly longer period than CH_4. In other words, when the CH_4 concentration decreases to 0 ppm, the CO_2 concentration is still very large at the same moment. This is because CH_4 is mainly produced from peat pyrolysis, and this reaction is weakened after the smoldering front reaches the bottom of the reactor. In contrast, CO_2 is mainly emitted from char oxidation which still exists based on the fact that the mass-loss rates in Fig. 9(a) are still larger than 1 g/min.

Fig. 10 shows the CH_4 and CO_2 emissions measured by TDLAS under

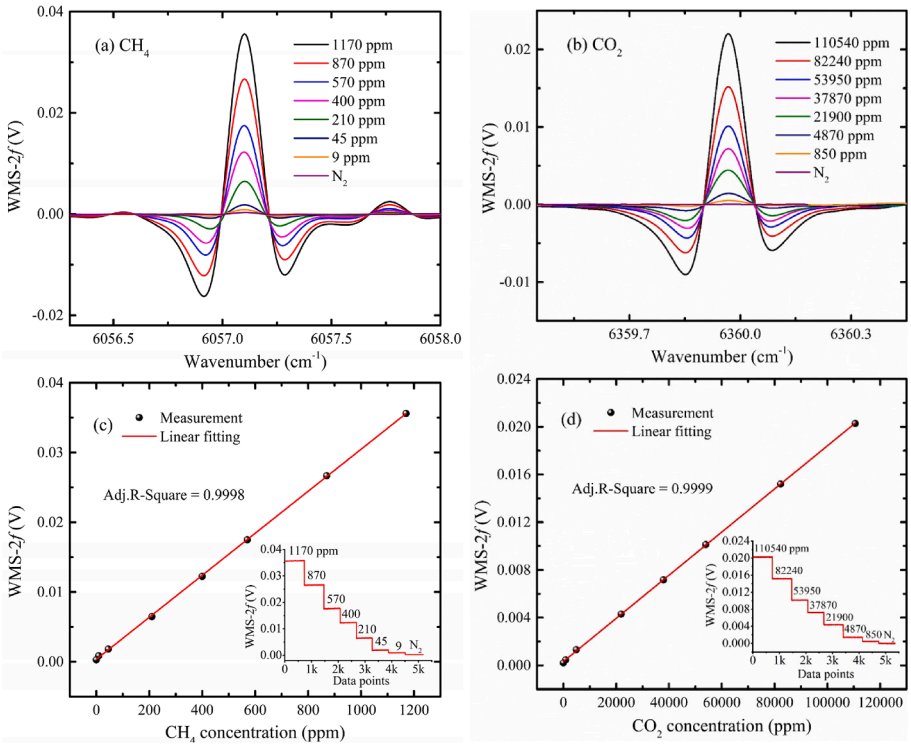

Fig. 5. Simultaneously recorded WMS-2*f* spectra of (a) CH_4 and (b) CO_2 at different gas concentrations, along with their corresponding linear calibration presented in (c) and (d), respectively.

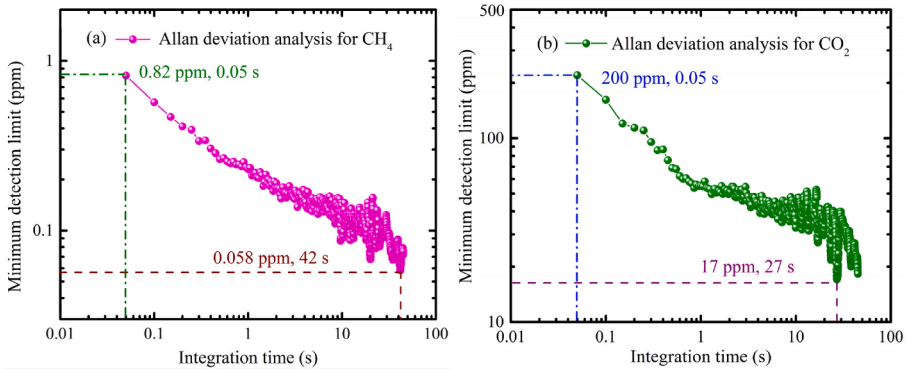

Fig. 6. Allan deviation plot for (a) CH_4 and (b) CO_2 as a function of integration time.

various peat moisture contents and at a constant airflow velocity of 27 mm/s. As the moisture content is increased, both the CH_4 and CO_2 emissions decrease significantly. This is partly attributed to the added water decreasing the dry mass of fuel and the swelling of the sample volume (decreasing dry peat bulk density with MC) [38].

4.3. Smoldering emission characteristics

Fig. 11 shows the peak and average CH_4/CO_2 ratios under different peat moisture contents and airflow velocities. It is important to highlight that measuring the concentration of a single gas is ineffective since it greatly depends on the location of measurement. However, utilizing the ratio of two gases can circumvent this issue according to the recent work by Wang et al. [39] and Chen et al. [40] by measuring the ratio of CH_4 (or VOCs) to CO_2 to quantify smoldering emissions. Therefore, we adopt the similar strategy by studying the CH_4/CO_2 ratio in this paper to avoid the influence of measurement location. The CH_4/CO_2 ratio helps characterize the competition between pyrolysis and oxidation reactions in smoldering combustion. As the pyrolysis of biomass generates more CH_4 than the oxidation of biomass and chars [8,9,41], an increased value of CH_4/CO_2 indicates the enhanced pyrolysis process or the weaker char oxidation.

As seen in Fig. 11(a), the average and peak CH_4/CO_2 ratios are generally lower than 0.08 and 0.15, respectively, under all tested conditions. Specifically, it is observed that the average CH_4/CO_2 ratio decreases from 0.06 to 0.043 as peat moisture content increases from 8% (dry peat) to 100%. As most of the CH_4 is produced in fuel pyrolysis [8,9,41], a higher fuel moisture content weakens the pyrolysis process thus reducing the CH_4 emission. On the other hand, the ratio of average CH_4/CO_2 increases with the oxygen supply from 0.053 (10 mm/s) to 0.075 (24 mm/s), because the stronger char oxidation increases the temperature and intensity of pyrolysis reactions.

CO_2 and CH_4 are two major GHGs emitted from peat smoldering fires [3]. Although N_2O is also regarded as a potent GHG, its amount from peat smoldering is very small which can be ignored here. Although CH_4 emission is found to be much smaller than CO_2, its global warming

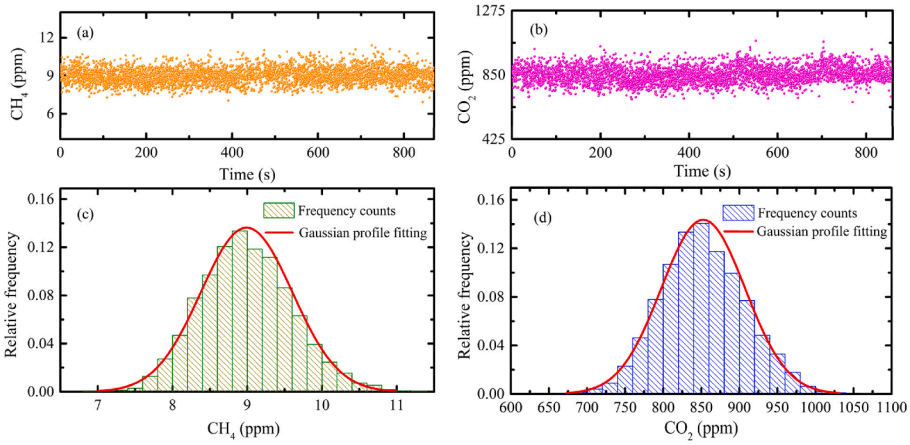

Fig. 7. Simultaneous continuous measurements of (a) 9 ppm CH_4 and (b) 850 ppm CO_2. The corresponding frequency distribution of (c) 9 ppm CH_4 and (d) 850 ppm CO_2 measurement is plotted along with the Gaussian fitting.

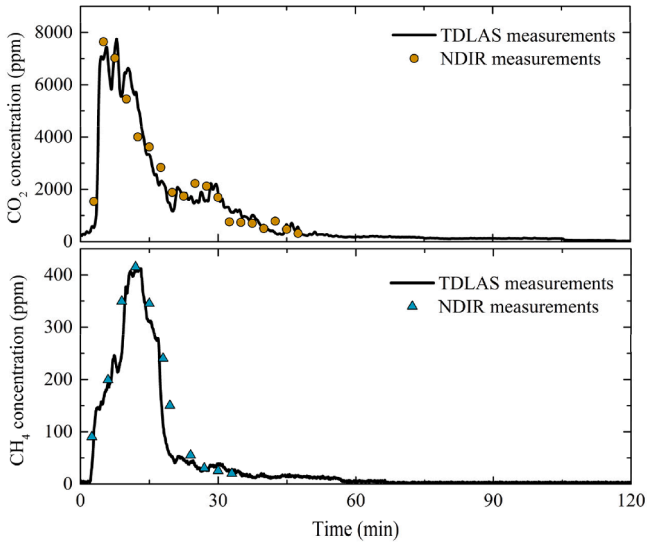

Fig. 8. Evolution of CO_2 and CH_4 concentrations at $u_{air} = 10$mm/s.

effects cannot be ignored. Herein, the GHGs from peat smoldering are simplified as a mixture of CO_2 and CH_4, and the equivalent GHG flux is estimated by [42]:

$$\dot{m}''_{GHG} = \frac{GWP_{CO_2}\Delta\dot{m}''_{CO_2} + GWP_{CH_4}\Delta\dot{m}''_{CH_4}}{GWP_{CO_2}} \tag{5}$$

where *GWP* is the global warming potential of the species. In practice, CO_2 is taken as the reference gas and given a 100-year *GWP* of 1, and GWP_{CH_4} is defined as 25 here [42]. Then, $\dot{m}''_{CO_2}$ and $\dot{m}''_{CH_4}$ are the emission fluxes of CO_2 and CH_4, which can be expressed as:

$$\dot{m}''_i = \frac{\rho_i \Delta X_i \dot{V} \times 10^{-3}}{A} \tag{6}$$

where ρ_i is the density of gas species i (kg/m^3), ΔX_i is the real-time concentration of the species i (ppm), $\dot{V}$ is the volume flow rate in the sampling duct, which is measured to be 1.7×10^{-3} m^3/s, and A is the cross-sectional area of the smoldering burner (m^2).

Fig. 12 (a) and (b) show the time-averaged $\dot{m}''_{CO_2}$ and $\dot{m}''_{CH_4}$ and the equivalent $\dot{m}''_{GHG}$ under different peat moisture contents and airflow rates, respectively. Both the moisture content and the airflow velocity have significant effects on the GHG flux. As expected, the equivalent

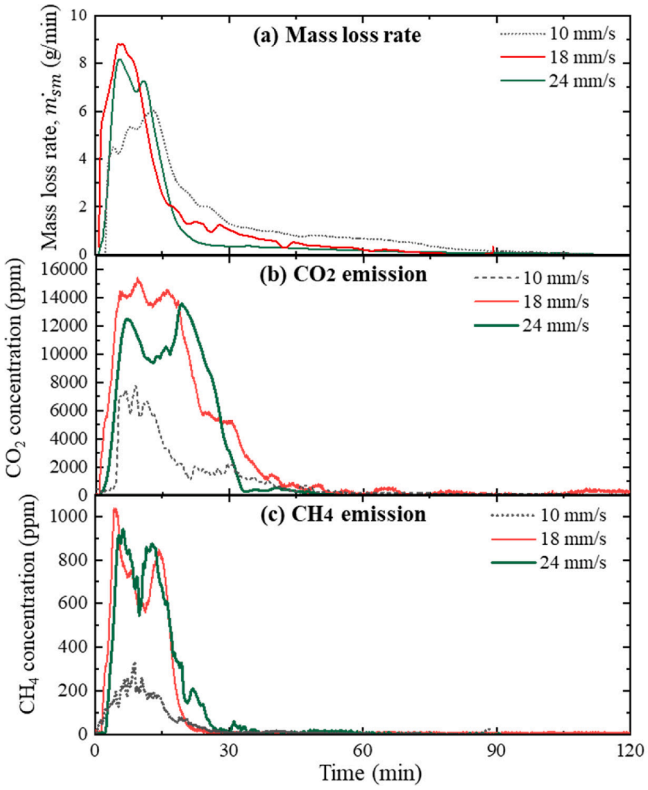

Fig. 9. Evolutions of the mass-loss rate, detected CH_4 and CO_2 emissions from dried peat smoldering under different airflow velocities.

$\dot{m}''_{GHG}$ decreases as the fuel moisture content increases, but it increases with the airflow velocity. For instance, the equivalent $\dot{m}''_{GHG}$ is 1.5 g/m^2·s under the airflow velocity of 10 mm/s, and it increases to about 3.4 g/m^2·s when the airflow velocity increases to 24 mm/s.

The average emission factor (EF_{av}, g/kg) for gas species is further calculated through Eq. (7) and shown in Fig. 12 (c):

$$EF_{av}(t) = \frac{\dot{m}''_{i-av}}{\dot{m}''_{sm-av}} \times 10^3 \tag{7}$$

where $\dot{m}''_{sm-av}$ (g/m^2•s) is the average smoldering flux (mass loss rate per unit area of the fuel), and $\dot{m}''_{i-av}$ (g/m^2•s) is the average emission flux of gas species i shown in Fig. 12 (b). As shown in Fig. 12 (c), the average

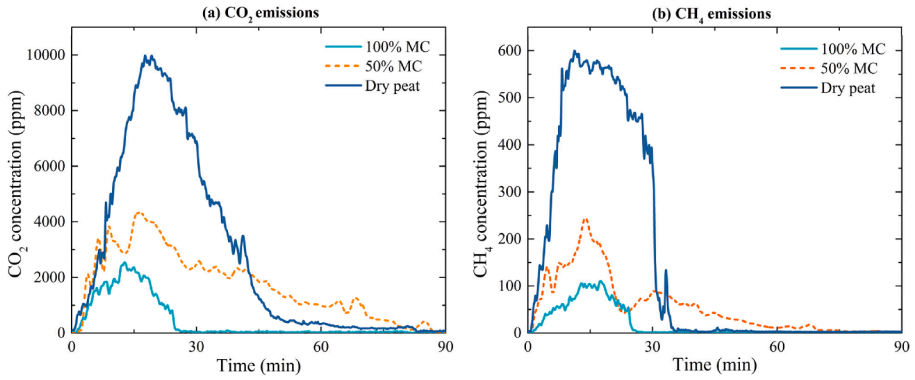

Fig. 10. Measured emissions of (a) CO_2 and (b) CH_4 under different peat moisture contents (u_{air} = 27 mm/s).

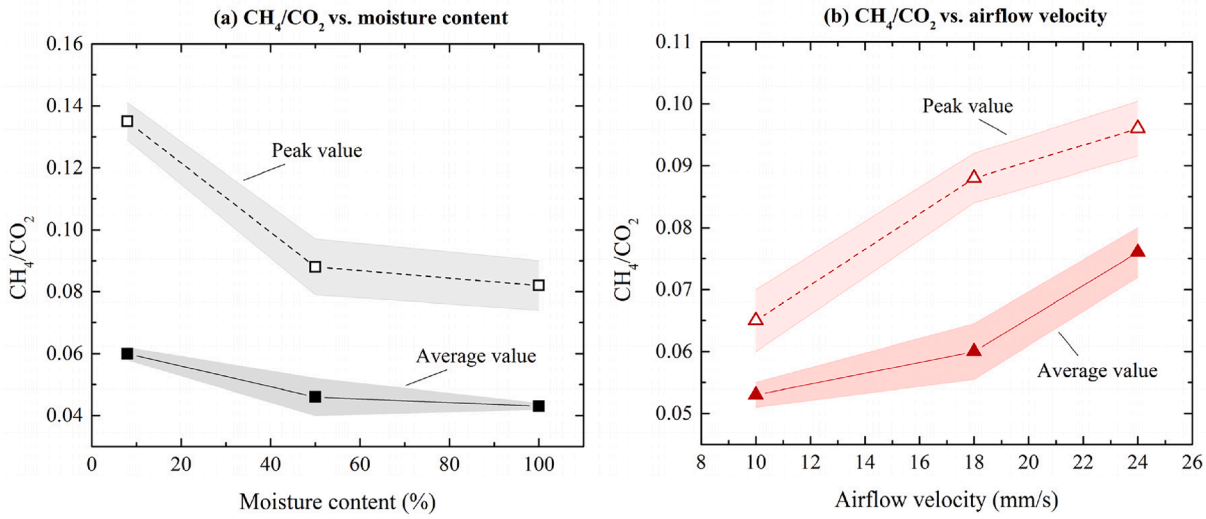

Fig. 11. Variation of CH_4/CO_2 ratio with (a) peat moisture content and (b) supplied airflow velocity. The clouds represent the uncertainty of repeated tests.

EFs of CH_4 are around 20 g/kg and increase with the airflow velocity. Comparatively, the average EFs of CO_2 and equivalent GHGs are significantly larger than that of CH_4. When the airflow velocity rises from 10 mm/s to 18 mm/s, the EF of GHG increases from 1008 to 1458 g/kg. But when the airflow velocity continues to increase to 24 mm/s, the EF of GHG increases slightly to about 1582 g/kg. Therefore, it can be concluded that the GHGs emitted from smoldering wildfires are significantly influenced by fuel and environmental conditions such as the weather, climate (dry or wet season), and the wind.

In summary, the detailed investigation discloses the capability of the developed dual-gas TDLAS sensor for simultaneously detecting CH_4 and CO_2 under various smoldering conditions. The TDLAS sensor has a promising potential to be used in smoldering fire detection and smoldering research to examine transient phenomena due to its superior time response.

5. Conclusions

A dual-gas optical sensor was developed using time-division multiplexed scanned wavelength modulation spectroscopy for peat fire detection by simultaneously measuring transient CH_4 and CO_2 emissions from a lab-scale smoldering peat combustion reactor. The sensor comprises two infrared lasers, an infrared photodetector, and a custom-designed Herriot multipass gas cell (10.3 m path length). Two infrared lasers operating at 1650 nm and 1572 nm were combined for exploiting CH_4 and CO_2 absorption lines centered at 6057.09 cm^{-1} and 6359.96 cm^{-1}, respectively. The injection current of 1572 nm and 1650 nm lasers was sinusoidally modulated at 15 kHz and 18 kHz with triangular scanned across the selected absorption lines of CH_4 and CO_2 at 10 Hz. A compact custom-designed Herriot multipass gas cell with an effective path length of 10.3 m in a volume of 40.5 mL was employed to improve detection sensitivity. Allan-Werle deviation analysis yielded the MDL of 0.058 ppm for CH_4 and 17 ppm for CO_2 at an optimum integration time of 42-s and 27-s, respectively. The simultaneous real-time measurements were recorded at an interval of 0.1 s to capture the transient CH_4 and CO_2 emissions under various smoldering peat fire conditions in a top-open cylinder reactor. The results agree well with the traditional commercial NDIR CO_2 and CH_4 analyzers. However, these commercial instruments show a slow time resolution of ~ 2.5 min and ~ 3 min, respectively, which is inadequate for measuring the transient change in peat fire emissions. The GHG flux and CH_4/CO_2 ratio increase from 1.5 g/m^2 s to 3.4 g/m^2 s and 0.053 to 0.075, respectively, with increasing oxygen supplies from 10 mm/s to 24 mm/s. However, the GHG flux and CH_4/CO_2 ratio decreased from 2.6 g/m^2 s to 0.4 g/m^2 s and 0.06 to 0.043 with the peat moisture content increased from 8% (dry peat) to 100%. The demonstrated time-division multiplexed dual-gas sensor offers a fast temporal resolution, high sensitivity, hardware simplicity, and compactness, which make it attractive for detecting transient emissions in underground peatland fires and monitoring overall GHG emissions from smoldering wildfires. Together with the state-of-the-art N_2O optical detector [43], future work will involve the simultaneous detection of the top three primary GHGs from smoldering biomass combustion.

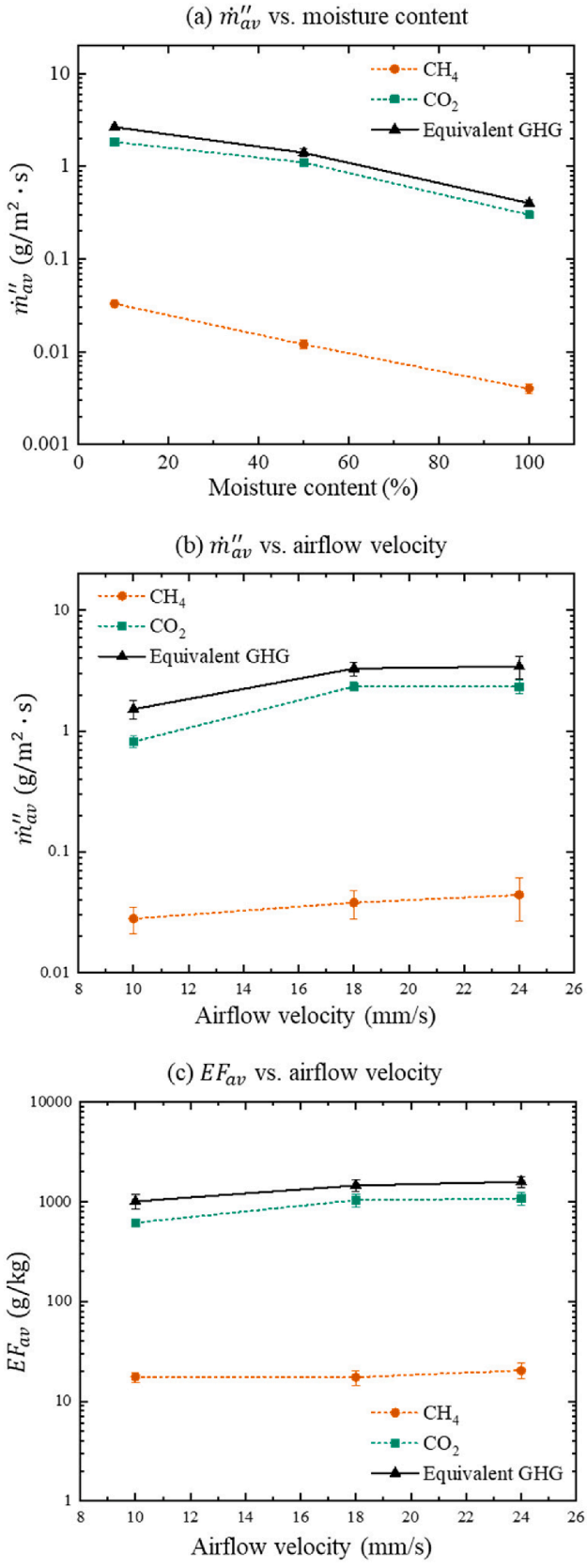

Fig. 12. Average equivalent GHG flux from peat smoldering versus (a) moisture content and (b) airflow velocity and (c) the average emission factors. The error bars (SE = $\sigma/\sqrt{n}$, where n = 2) shows the experimental uncertainty.

CRediT authorship contribution statement

Mohsin Raza: Conceptualization, Methodology, Investigation, Formal analysis, Validation, Visualization, Writing – original draft, Writing – review & editing. **Yuying Chen:** Methodology, Investigation, Formal analysis, Validation, Visualization, Writing – original draft, Writing – review & editing. **Joshua Trapp:** Methodology, Investigation. **Haojia Sun:** Methodology, Investigation. **Xinyan Huang:** Conceptualization, Methodology, Supervision, Writing – review & editing, Project administration, Funding acquisition. **Wei Ren:** Conceptualization, Methodology, Formal analysis, Validation, Visualization, Writing – review & editing, Supervision, Project administration, Funding acquisition.

Declaration of Competing Interest

The authors declare that they have no known competing financial interests or personal relationships that could have appeared to influence the work reported in this paper.

Data availability

Data will be made available on request.

Acknowledgments

This work is funded by National Natural Science Foundation of China (NSFC, 52122003 and 51876183), and Guangdong Science and Technology Department (2020A0505090010), China.

References

[1] Rein G. Smoldering combustion. In: Hurley MJ, Gottuk D, Hall JR, Harada K, Kuligowski E, Puchovsky M, editors. SFPE handbook of fire protection engineering. New York, NY: Springer, New York; 2016. p. 581–603.
[2] Rein G. Smouldering fires and natural fuels. In: Fire phenomena and the earth system; 2013. p. 15–33.
[3] Hu Y, Fernández Áñez N, Smith T, Rein G. Review of emissions from smouldering peat fires and their contribution to regional haze episodes. Internat J Wildland Fire 2018;27.
[4] Santoso MA, Christensen EG, Amin HMF, Palamba P, Hu Y, Purnomo DMJ, et al. GAMBUT field experiment of peatland wildfires in Sumatra: from ignition to spread and suppression. International Journal of Wildland Fire 2022.
[5] Hu Y, Rein G. Development of gas signatures of smouldering peat wildfires from emission factors. International J Wildland Fire 2022.
[6] Poulter B, Christensen Jr NL, Halpin PN. Carbon emissions from a temperate peat fire and its relevance to interannual variability of trace atmospheric greenhouse gases. J Geophys Res: Atmosph 2006:111(D6).
[7] Rein G, Huang X. Smouldering wildfires in peatlands, forests and the arctic: Challenges and perspectives. Current Opin Environ Sci Health 2021;24:100296.
[8] McMeeking GR, Kreidenweis SM, Baker S, Carrico CM, Chow JC, Collett Jr JL, et al. Emissions of trace gases and aerosols during the open combustion of biomass in the laboratory. Journal of Geophysical Research: Atmospheres 2009:114(D19).
[9] Hu Y, Fernandez-Anez N, Smith TEL, Rein G. Review of emissions from smouldering peat fires and their contribution to regional haze episodes. Internat J Wildland Fire 2018;27(5):293–312.
[10] Rein G. Smouldering combustion phenomena in science and technology. Internat Rev Chem Eng Jan 2009;1:3–18.
[11] Gerbreders V, Krasovska M, Mihailova I, Kostjukevics J, Sledevskis E, Ogurcovs A, et al. Metal oxide nanostructure-based gas sensor for carbon dioxide detection. Latv J Phys Tech Sci 2021;58(5):15–26.
[12] Yang W-B, Yuan C-S, Tong C, Yang P, Yang L, Huang B-Q. Diurnal variation of CO_2, CH_4, and N_2O emission fluxes continuously monitored in-situ in three environmental habitats in a subtropical estuarine wetland. Mar Pollut Bull 2017;119(1):289–98.
[13] Huang C-M, Yuan C-S, Yang W-B, Yang L. Temporal variations of greenhouse gas emissions and carbon sequestration and stock from a tidal constructed mangrove wetland. Mar Pollut Bull 2019;149:110568.
[14] Tsai C-P, Huang C-M, Yuan C-S, Yang L. Seasonal and diurnal variations of greenhouse gas emissions from a saline mangrove constructed wetland by using an in situ continuous GHG monitoring system. Environ Sci Pollut Res 2020;27(13):15824–34.
[15] Hsieh S-H, Yuan C-S, Ie I-R, Yang L, Lin H-J, Hsueh M-L. In-situ measurement of greenhouse gas emissions from a coastal estuarine wetland using a novel continuous monitoring technology: Comparison of indigenous and exotic plant species. J Environ Manage 2021;281:111905.

[16] Dinh T-V, Choi I-Y, Son Y-S, Kim J-C. A review on non-dispersive infrared gas sensors: Improvement of sensor detection limit and interference correction. Sens Actuators, B 2016;231:529–38.
[17] Yang J, Chen H, Zhao W, Zhou J. Combustion kinetics and emission characteristics of peat by using TG-FTIR technique. J Therm Anal Calorim 2016;124(1):519–28.
[18] Stockwell CE, Yokelson RJ, Kreidenweis SM, Robinson AL, DeMott PJ, Sullivan RC, et al. Trace gas emissions from combustion of peat, crop residue, domestic biofuels, grasses, and other fuels: configuration and Fourier transform infrared (FTIR) component of the fourth Fire Lab at Missoula Experiment (FLAME-4). Atmos Chem Phys 2014;14(18):9727–54.
[19] Hatch LE, Luo W, Pankow JF, Yokelson RJ, Stockwell CE, Barsanti KC. Identification and quantification of gaseous organic compounds emitted from biomass burning using two-dimensional gas chromatography–time-of-flight mass spectrometry. Atmos Chem Phys 2015;15(4):1865–99.
[20] Sengupta D, Samburova V, Bhattarai C, Watts AC, Moosmüller H, Khlystov AY. Polar semivolatile organic compounds in biomass-burning emissions and their chemical transformations during aging in an oxidation flow reactor. Atmos Chem Phys 2020;20(13):8227–50.
[21] Chow KK, Short M, Zeng H. A comparison of spectroscopic techniques for human breath analysis. Biomed Spectrosc Imaging 2012;1:339–53.
[22] Hu Y, Christensen E, Restuccia F, Rein G. Transient gas and particle emissions from smouldering combustion of peat. Proc Combust Inst 2019;37(3):4035–42.
[23] Farooq A, Alquaity ABS, Raza M, Nasir EF, Yao S, Ren W. Laser sensors for energy systems and process industries: Perspectives and directions. Prog Energy Combust Sci 2022;91:100997.
[24] Duan W, Yan F, Wang Y, Zhang H, Ma L, Wen D, et al. A Laser-Based Multipass Absorption Sensor for Sub-ppm Detection of Methane, Acetylene and Ammonia. Sensors 2022;22(2):556.
[25] Xu K, Zhao X, Wang Z, Chen J, Li T, Zheng Z, et al. Multipass-assisted dual-comb gas sensor for multi-species detection using a free-running fiber laser. Appl Phys B 2020;126(3):39.
[26] Hangauer A, Chen J, Strzoda R, Fleischer M, Amann MC. Fire detection with a compact, 2.3 μm VCSEL-based carbon monoxide sensor. In: Conference on lasers and electro-optics/international quantum electronics conference. Baltimore, Maryland: Optica Publishing Group; 2009. CTuA3 ..
[27] Fallows EA, Cleary TG, Miller JH. Development of a multiple gas analyzer using cavity ringdown spectroscopy for use in advanced fire detection. Appl Opt 2009;48 (4):695–703.
[28] Zheng F, Qiu X, Shao L, Feng S, Cheng T, He X, et al. Measurement of nitric oxide from cigarette burning using TDLAS based on quantum cascade laser. Opt Laser Technol 2020;124:105963.
[29] Qiu X, Wei Y, Li N, Guo A, Zhang E, Li C, et al. Development of an early warning fire detection system based on a laser spectroscopic carbon monoxide sensor using a 32-bit system-on-chip. Infrared Phys Technol 2019;96:44–51.
[30] Peng WY, Goldenstein CS, Mitchell Spearrin R, Jeffries JB, Hanson RK. Single-ended mid-infrared laser-absorption sensor for simultaneous in situ measurements of H_2O, CO_2, CO, and temperature in combustion flows. Appl Opt 2016;55(33): 9347–59.
[31] McManus JB, Zahniser M, Nelson D, Shorter J, Herndon S, Wood E, et al. Application of quantum cascade lasers to high-precision atmospheric trace gas measurements. Opt Eng 2010;49(11):111124.
[32] Goldenstein CS, Spearrin RM, Jeffries JB, Hanson RK. Infrared laser-absorption sensing for combustion gases. Prog Energy Combust Sci 2017;60:132–76.
[33] Sun K, Chao X, Sur R, Jeffries JB, Hanson RK. Wavelength modulation diode laser absorption spectroscopy for high-pressure gas sensing. Appl Phys B 2013;110(4): 497–508.
[34] Liu C, Xu L. Laser absorption spectroscopy for combustion diagnosis in reactive flows: A review. Appl Spectrosc Rev 2019;54(1):1–44.
[35] Gordon IE, Rothman LS, Hargreaves RJ, Hashemi R, Karlovets EV, Skinner FM, et al. The HITRAN2020 molecular spectroscopic database. J Quant Spectrosc Radiat Transfer 2022;277:107949.
[36] Cui R, Dong L, Wu H, Li S, Yin X, Zhang L, et al. Calculation model of dense spot pattern multi-pass cells based on a spherical mirror aberration. Opt Lett 2019;44 (5):1108–11.
[37] Giglio M, Patimisco P, Sampaolo A, Scamarcio G, Tittel FK, Spagnolo V. Allan deviation plot as a tool for quartz-enhanced photoacoustic sensors noise analysis. IEEE Trans Ultrason Ferroelectr Freq Control 2016;63(4):555–60.
[38] Huang X, Rein G. Downward spread of smouldering peat fire: the role of moisture, density and oxygen supply. Internat J Wildland Fire 2017;26(11):907–18.
[39] Wang H, van Eyk PJ, Medwell PR, Birzer CH, Tian ZF, Possell M, et al. Smouldering fire and emission characteristics of Eucalyptus litter fuel. Fire Mater 2022;46(3): 576–86.
[40] Chen Y, Lin S, Liang Z, Surawski NC, Huang X. Smouldering organic waste removal technology with smoke emissions cleaned by self-sustained flame. J Cleaner Prod 2022;362:132363.
[41] Yokelson RJ, Christian TJ, Karl TG, Guenther A. The tropical forest and fire emissions experiment: laboratory fire measurements and synthesis of campaign data. Atmos Chem Phys 2008;8(13):3509–27.
[42] Vallero DA. Air pollution calculations: quantifying pollutant formation, transport, transformation, fate and risks. first ed. Elsevier; 2019.
[43] Yang M, Wang Z, Nie Q, Ni K, Ren W. Mid-infrared cavity-enhanced absorption sensor for ppb-level N_2O detection using an injection-current-modulated quantum cascade laser. Opt Express 2021;29(25):41634–42.